III International Conference on Particle-based Methods – Fundamentals and Applications
PARTICLES 2013
M. Bischoff, E. Oñate, D.R.J. Owen, E. Ramm & P. Wriggers (Eds)

MESHFREE METHOD FOR COMPUTATIONAL AEROACOUSTICS USING LEE FOR THE SOLUTION OF NOISE PROPAGATION

JAROSLAV BAJKO[1], LIBOR ČERMÁK[1], MICHAEL HARTMANN[2] AND MIROSLAV JÍCHA[1]

[1] Faculty of Mechanical Engineering, Brno University of Technology
Technická 2896/2, 61669 Brno, Czech Republic
Email: y115413@stud.fme.vutbr.cz

[2] Volkswagen AG, Group Research
Letter Box 1777, D-38436 Wolfsburg, Germany

Key words: Acoustic pulse problem, computational aeroacoustics, Finite point method, linearized Euler equations

Abstract. Meshfree Finite point method (FPM) has been used for the solution of sound (noise) propagation, which can be modeled by linearized Euler equations (LEE). Important property of a numerical method for simulation of sound propagation is the capability to reach the high order of accuracy. In this paper we present the accuracy improvements of FPM using the reconstruction of variables in the Riemann solver by Taylor polynomial. Order of the derived meshfree method will be verified on 2D Acoustic pulse problem which serves as a benchmark problem with known analytical solution.

1 INTRODUCTION

Sound propagation problems form one specific group of problems within the computational aeroacoustics (CAA). Due to the aerodynamic and acoustic disparity, cf. [1], the numerical methods used in CAA have to reach high order of accuracy. Moreover, many engineering applications require the solution of governing equations for complex geometries. Some disadvantages of standart mesh-based methods can be overcome by meshfree methods, which do not require the mesh generation. Li, *et al.*, cf. [2], have already proposed a meshfree method for CAA. We have studied the properties of meshfree Finite point method proposed by E. Oñate, e.g. [3], for the solution of linearized Euler equations, which model the sound propagation. We have improved the accuracy of FPM using the reconstruction of variables in the Riemann solver by Taylor polynomial. 2D Acoustic puls problem proposed by Tam and Webb, cf. [4], has been used as a benchmark problem. The order of improved FPM was estimated using the convergence study for this problem.

2 2D LINEARIZED EULER EQUATIONS

Let $\mathbf{w}(\mathbf{x},t) = (\rho(\mathbf{x},t), u(\mathbf{x},t), v(\mathbf{x},t), p(\mathbf{x},t))^T$ denotes the primitive (physical) variables, i.e. the density, velocity components and pressure. These quantities can be decomposed into a *reference state* $\mathbf{w}_0(\mathbf{x})$ and a time dependent *fluctuating* part $\mathbf{w}'(\mathbf{x},t)$, cf. [1], [5] in the following way

$$\mathbf{w} = \begin{pmatrix} \rho \\ u \\ v \\ p \end{pmatrix} = \underbrace{\begin{pmatrix} \rho_0 \\ u_0 \\ v_0 \\ p_0 \end{pmatrix}}_{\mathbf{w}_0} + \underbrace{\begin{pmatrix} \rho' \\ u' \\ v' \\ p' \end{pmatrix}}_{\mathbf{w}'}, \quad \mathbf{x} = (x,y) \in \mathbb{R}^2,\ t > 0. \tag{1}$$

Assuming the uniform flow, the homogeneous 2D LEE in matrix form can be written as follows

$$\frac{\partial \mathbf{w}'}{\partial t} + \mathbb{A}_1(\mathbf{w}_0)\frac{\partial \mathbf{w}'}{\partial x} + \mathbb{A}_2(\mathbf{w}_0)\frac{\partial \mathbf{w}'}{\partial y} = \mathbf{0}, \tag{2}$$

where the Jacobian matrices $\mathbb{A}_1(\mathbf{w}_0)$, $\mathbb{A}_2(\mathbf{w}_0)$ are

$$\mathbb{A}_1(\mathbf{w}_0) = \begin{pmatrix} u_0 & \rho_0 & 0 & 0 \\ 0 & u_0 & 0 & \frac{1}{\rho_0} \\ 0 & 0 & u_0 & 0 \\ 0 & \gamma p_0 & 0 & u_0 \end{pmatrix}, \quad \mathbb{A}_2(\mathbf{w}_0) = \begin{pmatrix} v_0 & 0 & \rho_0 & 0 \\ 0 & v_0 & 0 & 0 \\ 0 & 0 & v_0 & \frac{1}{\rho_0} \\ 0 & 0 & \gamma p_0 & v_0 \end{pmatrix}, \tag{3}$$

where γ is the adiabatic index ($\gamma = 1.4$).

3 FINITE POINT METHOD

3.1 Basic notation

Definition 3.1 *Let $\Omega \subset \mathbb{R}^d$ ($d = 1, 2$ or 3 in practise) be the domain and Γ its boundary. We define the global cloud $\hat{\Omega}$ as a finite set of points from $\overline{\Omega}$ which discretizes the closed domain $\overline{\Omega}$. We write*

$$\hat{\Omega} = \{\mathbf{x}_i\}_{i=1}^n . \tag{4}$$

Next, for each point $\mathbf{x}_i$ we can assign a domain $\Omega_i \subset \mathbb{R}^d$ such that $\bigcup_{i=1}^n \Omega_i \supseteq \overline{\Omega}$, $\mathbf{x}_i \in \Omega_i$, i.e. the union of Ω_i creates the covering of set $\overline{\Omega}$.

Definition 3.2 *Let the global cloud of points $\hat{\Omega} = \{\mathbf{x}_i\}_{i=1}^n$ is given and let $r_i > 0$ determines an open ball Ω_i in $\mathbb{R}^d$. Then we define the i-th local cloud $\hat{\Omega}_i$ as a finite set*

$$\hat{\Omega}_i = \hat{\Omega} \cap \Omega_i = \hat{\Omega} \cap \left\{\mathbf{x} \in \mathbb{R}^d, \|\mathbf{x} - \mathbf{x}_i\| < r_i\right\}. \tag{5}$$

Similarly we write

$$\hat{\Omega}_i = \left\{\mathbf{x}_j^i\right\}_{j=1}^{n_i}, \tag{6}$$

where n_i is the number of points in the local cloud $\hat{\Omega}_i$. Moreover, the particular point $\mathbf{x}_i = \mathbf{x}_1^i$ is called the star point[1] *of the local cloud $\hat{\Omega}_i$.*

Figure 1 illustrates the mutual relationship between the global cloud, local cloud and star point.

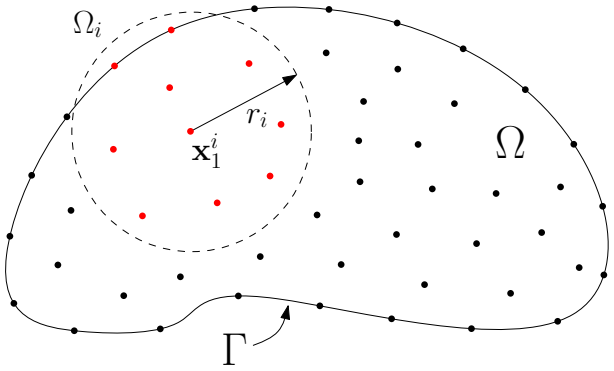

Figure 1: Domain Ω with boundary Γ, one particular domain Ω_i (open ball), star point $\mathbf{x}_1^i$, global cloud (black and red dots), local cloud corresponding to $\mathbf{x}_1^i$ (red dots).

3.2 Local approximation using WLSQ method

Consider a closed domain $\overline{\Omega}$ covered by n domains Ω_i and let $\hat{\Omega}_i = \left\{\mathbf{x}_j^i\right\}_{j=1}^{n_i}$ denotes the coresponding i-th local cloud. We wish to find the local approximation $\hat{w}_i : \Omega_i \to \mathbb{R}$ for each i-th local cloud $\hat{\Omega}_i$ in the form

$$\hat{w}_i(\mathbf{x}) = \sum_{l=1}^{m} \alpha_l^i p_l(\mathbf{x}) = \mathbf{p}^T(\mathbf{x})\boldsymbol{\alpha}_i, \quad i = 1, \ldots, n, \tag{7}$$

where

$$\boldsymbol{\alpha}_i = \left(\alpha_1^i, \alpha_2^i, \ldots, \alpha_m^i\right)^T \in \mathbb{R}^m \tag{8}$$

$$\mathbf{p}^T(\mathbf{x}) = \left(p_1(\mathbf{x}), p_2(\mathbf{x}), \ldots, p_m(\mathbf{x})\right). \tag{9}$$

Functions $p_l : \mathbb{R}^d \to \mathbb{R}$, $l = 1, \ldots, m$, form a basis $\mathcal{B}$ of a function space $\mathcal{F}$. In literature [6], [3], the *complete polynomial basis of degree* $\nu \in \mathbb{N}_0$ is proposed. For $d = 2$ and $\nu = 3$ we use e.g.

$$\mathcal{B} = \left\{1, x, y, x^2, xy, y^2, x^3, x^2y, xy^2, y^3\right\}. \tag{10}$$

[1]Star points $\mathbf{x}_i$ according (5) are centers of open balls Ω_i. For the sake of lucidity, the star point will be always written as the first point in explicit notation of a local cloud $\hat{\Omega}_i$.

Proposition 3.1 *Let* $\hat{\Omega}_i = \left\{\mathbf{x}_j^i\right\}_{j=1}^{n_i}$ *denotes the i-th local cloud and* $\mathbf{w}_i = \left(w_1^i, w_2^i, \ldots, w_{n_i}^i\right)^T$ *is the vector of function values prescribed at local cloud points* $\mathbf{x}_j^i$*. Moreover let the function basis* $\mathcal{B} = \{p_l(\mathbf{x});\, l = 1, 2, \ldots, m\}$ *is selected. Then the coefficients* $\boldsymbol{\alpha}_i$ *of the linear combination (7) can be obtained in the Weighted least squares sense as follows*

$$\boldsymbol{\alpha}_i = \mathbf{C}_i \mathbf{w}_i, \tag{11}$$

where

$$\mathbf{C}_i := \mathbf{A}_i^{-1}\mathbf{B}_i, \quad \mathbf{A}_i := \mathbf{P}_i^T \boldsymbol{\Phi}_i \mathbf{P}_i \quad \textit{and} \quad \mathbf{B}_i := \mathbf{P}_i^T \boldsymbol{\Phi}_i \tag{12}$$

are matrices of type $(m \times n_i)$*,* $(m \times m)$ *and* $(m \times n_i)$*, respectively. Matrix* $\mathbf{P}_i$ *of type* $(n_i \times m)$ *and diagonal matrix* $\boldsymbol{\Phi}_i$ *of order* n_i *is constructed as follows*

$$\mathbf{P}_i := \begin{pmatrix} \mathbf{p}^T(\mathbf{x}_1^i) \\ \mathbf{p}^T(\mathbf{x}_2^i) \\ \vdots \\ \mathbf{p}^T(\mathbf{x}_{n_i}^i) \end{pmatrix}, \quad \boldsymbol{\Phi}_i := \operatorname{diag}\left\{\phi_i(\mathbf{x}_j^i)\right\}_{j=1}^{n_i}, \tag{13}$$

where $\phi_i : \mathbb{R}^d \to \mathbb{R}$ *denotes a weighting function corresponding to the star point* $\mathbf{x}_1^i$*.*

3.3 Weighting function

Flexible weighting function $\phi_i(\mathbf{x})$ is the Gaussian-like function (cf. [3], [7]) given by 3 parameters (ω, k, γ) as follows

$$\phi_i(\mathbf{x}) = \frac{e^{-h^k} - e^{-\omega^k}}{1 - e^{-\omega^k}}, \quad \mathbf{x} \in \Omega_i \tag{14}$$

where $h := \dfrac{d\,\omega}{d_{\max}\,\gamma}$, $d := \|\mathbf{x}_1^i - \mathbf{x}\|$, $d_{\max} := \max\left\{\left\|\mathbf{x}_1^i - \mathbf{x}_j^i\right\|;\, j = 1, 2, \ldots, n_i\right\}$, $\mathbf{x}_j^i \in \hat{\Omega}_i$.

3.4 FPM for 2D Linearized Euler equations

Consider a domain $\Omega \subset \mathbb{R}^d$, $d = 2$, then the initial–value problem (IVP) for homogeneous LEE (2) written as a hyperbolic system reads

$$\text{(Hyperbolic PDE)} \qquad \frac{\partial \mathbf{w}}{\partial t} + \sum_{k=1}^{d} \frac{\partial \mathbf{F}_k(\mathbf{w})}{\partial x_k} = \mathbf{0}, \quad \mathbf{x} \in \Omega,\ t > 0 \tag{15}$$

$$\text{(IC)} \qquad \mathbf{w}(\mathbf{x}, 0) = \mathbf{w}_{\text{in}}(\mathbf{x}), \quad \mathbf{x} \in \Omega, \tag{16}$$

where $\mathbf{w} = (\rho', u', v', p')^T$ and the flux $\mathbf{F}_k(\mathbf{w}) = \mathbb{A}_k(\mathbf{w}_0)\mathbf{w}$.

Collocation (cf. [3]) of governing LEEs and stabilization of the scheme (cf. [8]) results in the initial–value problem for $\mathbf{w}_j^i(t) \approx \mathbf{w}(\mathbf{x}_j^i, t)$,

$$\text{(ODEs)} \qquad \sum_{j=1}^{n_i} \psi_j^i(\mathbf{x}_i) \frac{\partial \mathbf{w}_j^i(t)}{\partial t} = -2 \sum_{k=1}^{d} \sum_{j=2}^{n_i} \frac{\partial \psi_j^i}{\partial x_k}(\mathbf{x}_i) \left(\mathbf{F}_k^{ij+1/2} - \mathbf{F}_k^{i1} \right), \tag{17}$$

$$\text{(IC)} \qquad \mathbf{w}_j^i(0) = \mathbf{w}_{\text{in}}(\mathbf{x}_j^i), \quad \mathbf{x}_j^i \in \hat{\Omega}_i, \quad j = 1, \ldots, n_i, \quad i = 1, \ldots, n, \tag{18}$$

where $\mathbf{F}_k^{i1} := \mathbf{F}_k(\mathbf{w}_1^i(t))$ and $\mathbf{F}_k^{ij+1/2}$ is *a priory* unknown flux, cf. section 3.5. Moreover, the *shape functions* (cf. [6]) $\psi_j^i(\mathbf{x})$ are determined by WLSQ method as follows

$$\boldsymbol{\psi}_i^T(\mathbf{x}) = \left(\psi_1^i(\mathbf{x}), \psi_2^i(\mathbf{x}), \ldots, \psi_{n_i}^i(\mathbf{x}) \right) = \mathbf{p}^T(\mathbf{x}) \mathbf{C}_i. \tag{19}$$

The IVP (17, 18) has to be solved using a high order method, cf. section 4.5.

3.5 Midpoint flux

In this section we will show how to determine the desired flux components $\mathbf{F}_k^{ij+1/2}$, $k = 1, \ldots, d$ as a solution to the corresponding Riemann problem. This approach is known as the Godunov method, cf. [9].

Consider i-th local cloud $\hat{\Omega}_i$ with corresponding star point $\mathbf{x}_1^i$ and one particular neighbouring point $\mathbf{x}_j^i \in \hat{\Omega}_i$. Let us denote the vector connecting both points by $\mathbf{l}_{ij}$ and the corresponding unit vector by $\mathbf{n}_{ij} = (n_1^{ij}, n_2^{ij}, \ldots, n_d^{ij})$, i.e.

$$\mathbf{n}_{ij} = \frac{\mathbf{l}_{ij}}{\|\mathbf{l}_{ij}\|}, \quad \text{where} \quad \mathbf{l}_{ij} = \mathbf{x}_j^i - \mathbf{x}_1^i. \tag{20}$$

The flux $\mathbf{F}^{ij+1/2}$ represents the rate of flow from the star point $\mathbf{x}_1^i$ to its neighbour $\mathbf{x}_j^i$, so it can be obtained as an approximation of the directional flux $\tilde{\mathbf{F}}(\mathbf{w}) = \sum_{k=1}^{d} n_k^{ij} \mathbf{F}_k(\mathbf{w})$ in the direction $\mathbf{n}_{ij}$ at the point $\mathbf{x}_m^{ij} = \frac{1}{2}(\mathbf{x}_1^i + \mathbf{x}_j^i)$.

Proposition 3.2 *Let $\hat{\mathbf{w}}_j^i(t)$ be an approximation of the unknown function $\mathbf{w}(\mathbf{x}, t)$ at points $\mathbf{x}_j^i$ for $j = 1, \ldots, n_i$, $i = 1, \ldots, n$. Then the flux components $\mathbf{F}_k^{ij+1/2}$ can be obtained as*

$$\mathbf{F}_k^{ij+1/2} = \tilde{\mathbf{F}}(\mathbf{w}) n_k^{ij}, \tag{21}$$

where $\mathbf{w}$ is the solution to the Riemann problem $\mathcal{R}(\hat{\mathbf{w}}_1^i(t), \hat{\mathbf{w}}_j^i(t))$, i.e.

$$\frac{\partial \mathbf{w}}{\partial \tilde{t}} + \frac{\partial \tilde{\mathbf{F}}(\mathbf{w})}{\partial \tilde{x}} = \mathbf{0}, \quad \mathbf{w}(\tilde{x}, 0) = \begin{cases} \hat{\mathbf{w}}_1^i(t) & , \tilde{x} < 0 \\ \hat{\mathbf{w}}_j^i(t) & , \tilde{x} > 0, \end{cases} \tag{22}$$

at $\tilde{x} = 0$.

Approximations $\hat{\mathbf{w}}_j^i(t)$ can be chosen in different ways. The most natural choice for $\hat{\mathbf{w}}_j^i(t)$ is to evaluate the local approximations $\hat{\mathbf{w}}^i(\mathbf{x}, t)$, cf. (7), at their star points $\mathbf{x}_1^i$.

3.6 Reconstruction of variables

The reconstruction of variables means replacing the left and right state involved in the Riemann problem (22) by more accurate approximations. If we denote the reconstructed left state by $\mathbf{w}_j^+(t)$ and right state by $\mathbf{w}_j^-(t)$, then the IC (22) acquires the form

$$\mathbf{w}(\tilde{x},0) = \begin{cases} \mathbf{w}_1^+(t) & , \tilde{x} < 0 \\ \mathbf{w}_j^-(t) & , \tilde{x} > 0. \end{cases} \tag{23}$$

We recommend the reconstruction of variables (cf. [10], [11]) by means of the Taylor polynomial $\mathcal{T}_\nu(\mathbf{x})$ of degree $\nu \in \mathbb{N}_0$ evaluated at midpoints $\mathbf{x}_m^{ij}$. Derivatives are obtained from local approximations $\hat{\mathbf{w}}^i(\mathbf{x},t)$, cf. (7), evaluated at corresponding star point $\mathbf{x}_1^i$.

Consider i-th local cloud $\hat{\Omega}_i = \left\{\mathbf{x}_j^i\right\}_{j=1}^{n_i}$ which consists of the star point $\mathbf{x}_1^i$ and its neighbours $\mathbf{x}_j^i$, $j = 2.\ldots,n_i$. Midpoints of line segments connecting the star point with its neighbours are denoted by $\mathbf{x}_m^{ij}$. We will focus on the reconstruction for one pair of points: star point $\mathbf{x}_1^i$ and its neighbour $\mathbf{x}_j^i$ which has its own local cloud $\hat{\Omega}_k = \left\{\mathbf{x}_l^k\right\}_{l=1}^{n_k}$, $\mathbf{x}_1^k = \mathbf{x}_j^i$. Then we can construct $\mathbf{w}_1^+(t)$, $\mathbf{w}_j^-(t)$ as follows

$$\mathbf{w}_1^+(t) = \mathcal{T}_\nu^i(\mathbf{x}_m^{ij}) = \sum_{|\boldsymbol{a}|\le\nu} \frac{(\mathbf{x}_m^{ij} - \mathbf{x}_1^i)^{\boldsymbol{a}}}{\boldsymbol{a}!} \frac{\partial^{|\boldsymbol{a}|}}{\partial \mathbf{x}^{\boldsymbol{a}}} \hat{\mathbf{w}}^i(\mathbf{x}_1^i,t), \tag{24}$$

where $\boldsymbol{a} = (a_1,a_2,\ldots,a_d) \in \mathbb{N}_0^d$ is the multi–index. Value $\mathbf{w}_1^+(t) \approx \mathbf{w}^i(\mathbf{x}_m^{ij},t)$ using the local cloud $\hat{\Omega}_i$.

Similarly,

$$\mathbf{w}_j^-(t) = \mathcal{T}_\nu^k(\mathbf{x}_m^{ij}) = \sum_{|\boldsymbol{a}|\le\nu} \frac{(\mathbf{x}_m^{ij} - \mathbf{x}_j^i)^{\boldsymbol{a}}}{\boldsymbol{a}!} \frac{\partial^{|\boldsymbol{a}|}}{\partial \mathbf{x}^{\boldsymbol{a}}} \hat{\mathbf{w}}^k(\mathbf{x}_j^i,t). \tag{25}$$

Value $\mathbf{w}_j^-(t) \approx \mathbf{w}^k(\mathbf{x}_m^{ij},t)$ using the local cloud $\hat{\Omega}_k$.

Values $\mathbf{w}_1^+(t)$, $\mathbf{w}_j^-(t)$ vary depending on the degree ν of the Taylor polynomial. Of course, the reconstruction is limited by the basis $\mathcal{B}$. If we consider a complete polynomial basis of degree m, then the Taylor polynomial of degree $\nu \le m$ can be constructed.

Definition 3.3 *The reconstruction of variables $\mathbf{w}^+$, $\mathbf{w}^-$ required in the Riemann problem $\mathcal{R}(\mathbf{w}^+,\mathbf{w}^-)$ is said a ν–order reconstruction if the values $\mathbf{w}^+$, $\mathbf{w}^-$ are obtained using the Taylor polynomial of degree ν.*

Let $\mathcal{B}$ be the complete polynomial basis of degree $m = 3$, e.g. (10). Keeping in mind the notation used in (24, 25), then the 0–order reconstruction reads as

$$\mathbf{w}_1^+(t) = \mathcal{T}_0^i(\mathbf{x}_m^{ij}) = \hat{\mathbf{w}}^i(\mathbf{x}_1^i,t), \quad \mathbf{w}_j^-(t) = \mathcal{T}_0^k(\mathbf{x}_m^{ij}) = \hat{\mathbf{w}}^k(\mathbf{x}_1^k,t). \tag{26}$$

The 0–order reconstruction coincides with the natural choice mentioned earlier, i.e. we evaluate the local approximations $\hat{\mathbf{w}}^i(\mathbf{x}, t)$ at their star points.

Example 3.1 *Following example shows local approximations $\hat{w}^i(x,t)$, $\hat{w}^k(x,t)$ and Taylor polynomials $\mathcal{T}^i_\nu(x)$, $\mathcal{T}^k_\nu(x)$ which are constructed on 1D domains Ω_i and Ω_k. Both local clouds $\hat{\Omega}_i$ and $\hat{\Omega}_k$ consist of five points.*

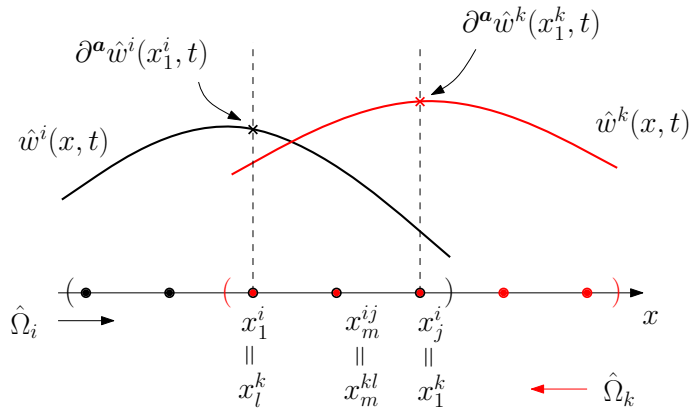

Figure 2: Local approximations $\hat{w}^i(\mathbf{x}^{ij}_m, t)$, $\hat{w}^k(\mathbf{x}^{kl}_m, t)$ on domains Ω_i, Ω_k, respectively.

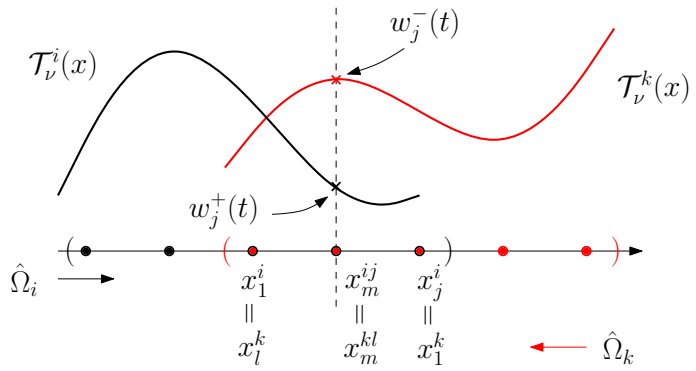

Figure 3: Taylor polynomials $\mathcal{T}^i_\nu(x)$, $\mathcal{T}^k_\nu(x)$ corresponding to domains Ω_i, Ω_k.

4 SIMULATION

4.1 2D Acoustic pulse problem

2D acoustic pulse problem is the initial–value problem given by the homogeneous 2D LEE (2) and the initial condition corresponding to the Gaussian acoustic, vorticity and entropy puls[2]. This problem was proposed by Tam and Webb in [4].

[2]Fourier analysis of the LEE shows that this equation system enables the propagation of three different waves - acoustic, vorticity and entropy wave. We refer the reader to [1] for further detail.

Consider IVP given by

$$\text{(PDE)} \qquad \frac{\partial \mathbf{w}'}{\partial t} + \mathbb{A}_1(\mathbf{w}_0)\frac{\partial \mathbf{w}'}{\partial x} + \mathbb{A}_2(\mathbf{w}_0)\frac{\partial \mathbf{w}'}{\partial y} = \mathbf{0}, \quad (x,y) \in \mathbb{R}^2,\ t > 0, \tag{27}$$

$$\text{(IC)} \qquad \mathbf{w}'(x,y,0) = \mathbf{w}'_{\text{in}}(x,y), \quad (x,y) \in \mathbb{R}^2. \tag{28}$$

The initial condition is prescribed as the superposition of the acoustic and vorticity puls, both located at point $(x_a, y_a) \in \mathbb{R}^2$ and the entropy puls located at point $(x_e, y_e) \in \mathbb{R}^2$. Written in compact form, the IC reads as

$$\mathbf{w}'_{\text{in}}(x,y) = \begin{pmatrix} \varepsilon_1 e^{-\kappa_1 r_a^2} + \varepsilon_2 e^{-\kappa_2 r_e^2} \\ \varepsilon_3 (y - y_a) e^{-\kappa_3 r_a^2} \\ -\varepsilon_3 (x - x_a) e^{-\kappa_3 r_a^2} \\ \varepsilon_1 e^{-\kappa_1 r_a^2} \end{pmatrix}, \tag{29}$$

where $r_a = \sqrt{(x-x_a)^2 + (y-y_a)^2}$ and $r_e = \sqrt{(x-x_e)^2 + (y-y_e)^2}$. Parameters ε_j, $\kappa_j = \dfrac{\ln 2}{b_j^2}$, b_j, $j = 1,2,3$, determine the amplitude and the half–width of the acoustic, vorticity and entropy puls, respectively.

We assume the subsonic uniform mean flow in x-direction, i.e. we prescribe the vector $\mathbf{w}_0 = (\rho_0, u_0, v_0, p_0)^T$ as follows

$$\rho_0 = 1, \quad u_0 = 0.5, \quad v_0 = 0, \quad p_0 = \frac{\rho_0}{\gamma} = \frac{5}{7}. \tag{30}$$

Then the reference speed of sound a_0 and the Mach number M_0 will be also constant and take the values

$$a_0 = \sqrt{\frac{\gamma p_0}{\rho_0}} = 1 \quad \text{and} \quad M_0 = 0.5. \tag{31}$$

4.2 Analytical solution

We utilize the analytical solution to the 2D Acoustic pulse problem for convergence study in section 4.6. The rigorous derivation can be found in [4], appendix A.

4.3 Numerical solution

Let us choose a bounded domain $\Omega = (-24, 24) \times (-24, 24)$. We prescribe the center of initial acoustic and vorticity puls at point $(x_a, y_a) = (-9, 0)$, while the center of initial entropy puls is moved to the point $(x_e, y_e) = (0, 9)$. The parameters of each puls are summarized in Table 1.

Table 1: Parameters ε_j and b_j used in IC (29).

ε_1	=	0.01	$b_1 = 3$
ε_2	=	0.002	$b_2 = 3$
ε_3	=	0.0008	$b_3 = 3$

The acoustic waves propagate with the speed of sound $a_0 = 1$ in all directions and moreover they are convected with the velocity $u_0 = 0.5$. In order to avoid the interaction with the boundary of Ω, we will compute just to time $T = 10$. Let us describe the spatial and time discretization.

The domain Ω and the initial condition is depicted schematically in Fig. 4.

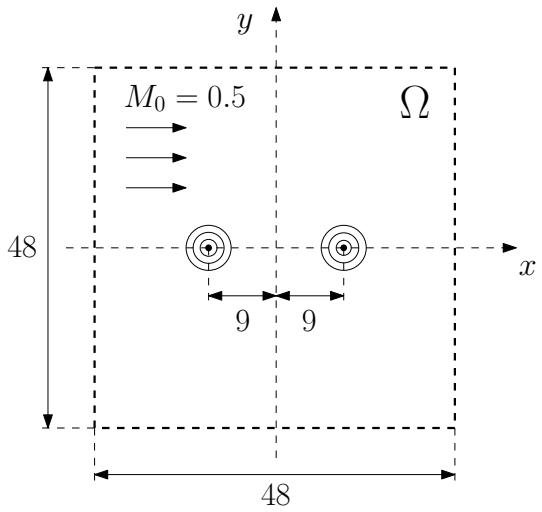

Figure 4: Bounded domain Ω and the initial condition.

4.4 Spatial discretization

Let h denotes the spatial step in x-direction and y-direction. Thus, the uniform discretization of the domain Ω is adopted. We will compute the solution for four spatial steps $h = 1, 0.8, 0.6, 0.4$ and corresponding global clouds will therefore consist of $2401, 3721, 6561, 14641$ points, respectively. Next, we choose the basis $\mathcal{B}$ as the complete polynomial basis of degree 3, cf. (10). Basis consists of $m = 10$ functions, i.e. each local cloud $\hat{\Omega}_i$, $i = 1, \ldots, n$, has to contain minimally 10 points. Initial search radius $r_i = 3.30h$ is chosen for each point $\mathbf{x}_i \in \hat{\Omega}$. Weighting function parameters were chosen as $(\omega, k, \gamma) = (3.1, 2, 1.01)$, cf. section 3.3.

4.5 Time discretization

Due to the solution of linear problem (linearized Euler equations), we can utilize the 5–stage LDDRK, cf. [12], which can be implemented using 2 storages only,

$$\mathbf{K}_l = \Delta t\, \mathbf{F}(\mathbf{U}^k + a_l \mathbf{K}_{l-1}), \quad l = 1, \ldots, 5, \tag{32}$$

$$\mathbf{U}^{k+1} = \mathbf{U}^k + \mathbf{K}_5, \tag{33}$$

where the coefficients a_l are listed in Table 2. The time step Δt is chosen with respect to the spatial step and the mean flow as $\Delta t = h/(1 + M_0)$, cf. [5].

Table 2: Coefficients for low storage implementation, cf. [12], p. 182, 185.

a_1	a_2	a_3	a_4	a_5
0	0.19771897	0.23717924	0.33311600	0.5

4.6 Convergence study

Table 3 contains the comparison between analytical and numerical solution for density measured by the maximal absolute error $E_{\max}$

$$E_{\max} = \max\left\{|\rho'^i(T) - \rho'(x_i, y_i, T)|;\ i = 1, \ldots, n\right\} \tag{34}$$

for different spatial discretizations and ν-order reconstruction of variables. The maximal absolute error in Table 3 was computed only at points $y_i = 0$ and at time $T = 10$.

Table 3: Maximal error using ν–order reconstruction.

$E_{\max}$	2401 p. ($h = 1$)	3721 p. ($h = 0.8$)	6561 p. ($h = 0.6$)	14641 p. ($h = 0.4$)
$\nu = 0$	8.664×10^{-4}	7.782×10^{-4}	6.745×10^{-4}	5.422×10^{-4}
$\nu = 1$	2.050×10^{-4}	1.064×10^{-4}	4.526×10^{-5}	1.320×10^{-5}
$\nu = 2$	4.698×10^{-5}	3.140×10^{-5}	1.728×10^{-5}	6.231×10^{-6}
$\nu = 3$	3.226×10^{-5}	1.577×10^{-5}	7.117×10^{-6}	1.168×10^{-6}

The logarithm of the error $\ln(E_{\max})$ was depicted over $\ln(h)$ for each ν. We have fitted the line through obtained points for each reconstruction. The slopes of these fitted lines provide an estimate of FPM order. Namely, for the ν–order reconstruction, $\nu = 0, 1, 2, 3$, we have obtained the slopes 0.51, 2.99, 2.21, 3.58, respectively.

The most accurate results were obtained using the 3–order reconstruction. In this case, the FPM reaches almost 4-th order (experimental order) of accuracy.

Figures 5, 6 show the acoustic density $\rho'(x, y, T)$, $T = 10$ at points $y = 0$ for the uniform discretization of 2401 points ($h = 1$) and for different reconstruction of variables. The analytical solution is depicted as the solid line.

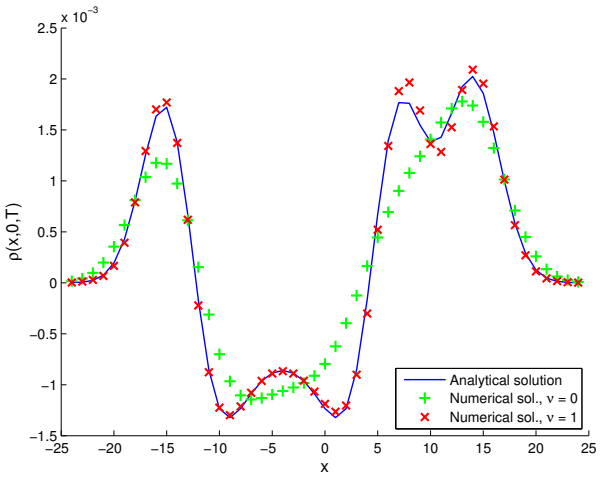

Figure 5: Comparison between zero– and first–order reconstruction.

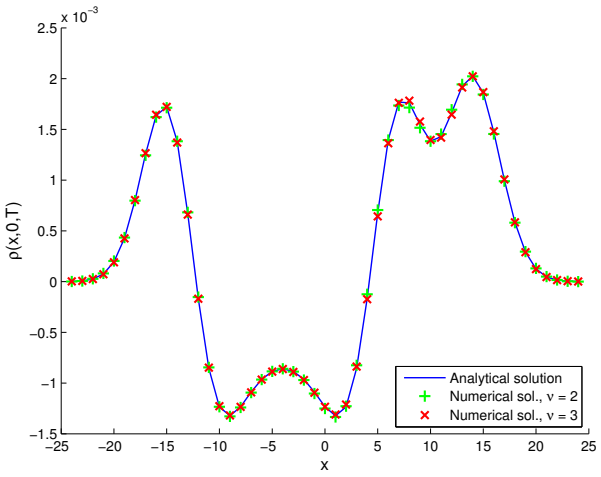

Figure 6: Comparison between second– and third–order reconstruction.

5 CONCLUSION

We have solved the IVP (27, 28) in order to study the accuracy of FPM for different reconstruction of variables involved in the Riemann problem, cf. (22). We have utilized the knowledge of analytical solution for comparison of obtained results, which were used to estimate the order of FPM, cf. section 4.6. Clearly, for complete polynomial basis of degree 3, the highest accuracy (FPM of order 4) was obtained using the 3–order reconstruction.

REFERENCES

[1] Roeck W.D.: *Hybrid Methodologies for the computational Aeroacoustic Analysis of Confined, Subsonic Flows*, doctoral thesis, Katholieke Universiteit Leuven, ISBN 978-90-5682-803-5, 2007.

[2] Li K., Huang Q.B., Wanga J.L., Lin L.G.: *An improved localized radial basis function meshless method for computational aeroacoustics*, Engineering Analysis with Boundary Elements 35, 47–55, 2011.

[3] Ortega E., Oñate E., Idelsohn S.: *A Finite point method for adaptive three-dimensional compressible flow calculations*, Int. J. Numer. Meth. Fluids, 60:937–971, 2009.

[4] Tam Ch.K.W., Webb J.C.: *Dispersion-Relation-Preserving Finite Difference Schemes for Computational Acoustics*, Journal of Computational Physics 107, 262–281, 1993.

[5] Bailly Ch., Juvé D.: *Numerical Solution of Acoustic Propagation Problems Using Linearized Euler Equations*, AIAA Journal Vol. 38, No. 1, January 2000.

[6] Liu G.R., Gu Y.T.: *An Introduction to Meshfree Methods and Their Programming*, Springer Berlin, ISBN 10 1-4020-3468-7, 2005.

[7] Ortega E., Oñate E., Idelsohn S.: *An improved Finite point method for tridimensional potential flows*, Comput Mech, 40:949–963, 2007.

[8] Katz A., Jameson A.: *Edge-based Meshless Methods for Compressible Flow Simulations*, AIAA Paper 2008-699, 46th AIAA Aerospace Sciences Meeting and Exhibit, Reno, Nevada, USA, January 2008.

[9] Toro E.F.: *Riemann Solvers and Numerical Methods for Fluid Dynamics*, 2nd Edition Springer-Verlag, ISBN 3-540-65966-8, 1999.

[10] Nogueira X., Khelladi S., Colominas I., Cueto-Felgueroso L., París J., Gómez H.: *High–resolution Finite volume methods on unstructured grids for turbulence and aeroacoustics*, Archives of Computational Methods in Engineering, 18:315–340, 2011.

[11] Cueto-Felgueroso L., Colominas I.: *High–order Finite Volume Methods and Multiresolution Reproducing Kernels*, Arch Comput Methods Eng 15:185–228, 2008.

[12] Hu F.Q., Hussainy M.Y., Manthey J.L.: *Low–Dissipation and Low–Dispersion Runge–Kutta Schemes for Computational Acoustics* , Journal of Computational Physics 124, 177-191, Article No. 0052, 1996.